A Mg-In Alloy Interphase for Mg Dendrite Suppression

To cite this article: Brian C. Lee and Kimberly A. See 2024 *J. Electrochem. Soc.* **171** 010513
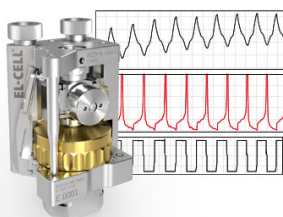
View the article online for updates and enhancements.

CrossMark

A Mg-In Alloy Interphase for Mg Dendrite Suppression

Brian C. Lee ⬡ and Kimberly A. See ⬡*,z

Division of Chemistry and Chemical Engineering, California Institute of Technology, Pasadena, California 91125, United States of America

Mg metal batteries have attracted much attention as an alternative to Li-ion technology due to the high abundance and volumetric capacity of Mg metal. Further, early reports show that Mg is less prone to dendritic growth compared to Li, thereby improving the safety and long-term reversibility of Mg metal anodes. However, dendritic growth of Mg can be observed in various conditions, causing cell shorting and capacity loss. Herein, we report a chemically-formed Mg-In alloy interphase that suppresses nonuniform Mg growth during electrochemical reduction. Ex-situ X-ray diffraction shows that upon reduction, Mg alloys into the Mg-In interphase with no evidence of Mg deposition on top of the surface during initial cycles. Interestingly, further reduction results in Mg depositing underneath the interphase, which confirms Mg mobility through the interphase. However, the alloying reaction is kinetically limited, leading to significant Mg deposition on top of the interphase at high current densities. Thus, alloys on Mg can affect deposition morphologies, but are limited by the kinetics of Mg conduction through the alloy.
© 2024 The Electrochemical Society ("ECS"). Published on behalf of ECS by IOP Publishing Limited. [DOI: 10.1149/1945-7111/ad1c13]

Mg batteries have been studied as a promising alternative to current Li-ion battery technology due to high natural abundance and well-dispersed deposits of Mg-containing precursors.[1] However, Mg batteries are only competitive from a performance perspective if a Mg metal anode is used. Mg metal anodes have a very high volumetric capacity of 3833 mAh cm^{-3} and a reasonable gravimetric capacity of 2295 mAh g^{-1}, but face a host of challenges that prevent commercialization. One of the biggest challenges facing Mg metal is the tendency for Mg metal to passivate by reaction with water, oxygen, and other electrolyte components to form an insulating layer, shutting down deposition and stripping of the metal.[2–6] As such, research into Mg metal anodes initially consisted primarily of investigation into electrolytes to control the interface and prevent the passivation of the Mg metal surface. To that end, several classes of electrolytes, such as those based on Grignard reagents,[5,7–12] halide-containing electrolytes,[13–18] trifluoromethanesulfonimide (TFSI) salts,[19–21] fluorinated weakly coordinating anions,[22,23] and boron hydride-based anions[24,25] were developed to varying degrees of success.

A potential attractive feature of Mg metal anodes is the smooth deposition morphology compard to Li metal. Matsui observed that at the same current densities (2.0 mA cm^{-2}), Li forms dendrites while Mg deposits in plate-like morphologies.[26] The lower self-diffusion barrier of Mg compared to Li was hypothesized to result in smoother morphologies.[27] Control over metal deposition morphology is crucial as dendrites can have many detrimental effects, such as capacity fade as a result of dead metal or shorting of the cell when the dendrites pierce through the separators, posing safety hazards associated with thermal ruanway in the presence of a flammable electrolyte.[28] However, despite the low self-diffusion barrier inherent to Mg metal, the kinetics of the electron transfer coupled with mass transport limitations can outpace the self-diffusion at high enough current density. During deposition, the metal cations nucleate and deposit until the ions at the surface of the negatively charged electrode deplete.[29–31] The anions are repelled from the cathode, while the cations are consumed, causing a large space charge region at the electrode. As a result of the space charge region, the cations deposit in such a way to maximize growth toward the anode to minimize the space charge build up, causing dendritic morphologies.[30] As such, dendritic growth of Mg has been reported in literature. Davidson et al. observed Mg dendrites at 0.921 mA cm^{-2}, which is a lower current density than Matsui

reported.[32] However, the growth was mostly observed at the edges of a Mg ribbon, where higher local flux would occur. Eaves-Rathert et al. also observed nonuniform growth of Mg at 0.2 mA cm^{-2} in a coin cell geometry using a polymer separator. While the Mg deposits are not dendritic in the classic sense that the deposits do not form classic branching structures, hemispherical islands form using the separator as scaffolding and stack on top of each other to form deposits that cause shorts through the polymer separator.[33] The deposits are referred to as 3D growth but cause the same harmful effects as a classic dendrite would. The separator scaffolding effect is also observed by Hebié et al. and Ding et al.[34–36]

A strategy to suppress Mg dendrites is through modification of the electrode surface. The formation of artificial interphases on Mg surfaces has been commonly employed to improve Mg cycling by protecting the anode from passivation.[37,38] However, some interphases, particularly alloy-based systems, have been noted in literature to minimize dendrites as well. Several different mechanistic explanations have been given for the dendrite-reducing ability of alloy interphases. In many alloy interphase systems, the alloy interphase decreases insulating passivation with the electrolyte, which prevents preferential deposition at localized points with low electrical resistance. As such, a smoother Mg morphology on the electrode is observed.[39–42]

Of particular interest are two alloy interphase systems where the Mg is hypothesized to conduct through the alloy interphase and deposit underneath. A Mg|Mg-Sn electrode was shown to decrease Mg stripping and deposition overpotential while maintaining fast kinetics, exhibiting <1 V overpotentials at a very high current density of 6 mA cm^{-2} in symmetric cells. The Mg deposits at the Mg|Mg-Sn interface is observed by cross-section scanning electron microscopy (SEM). The bulk composition of the alloy remains unchanged through cycling by X-ray photoelectron spectroscopy (XPS), indicating mobility of Mg through the Mg-Sn interphase and depositing underneath at the Mg|Mg-Sn interface. However, the study focused mainly on cycling stability, and the mechanism of the electroreduction process in the interphase was not determined.[43]

In a Mg-Ga alloy interphase system, shorts when cycling in a symmetric cell were prevented when using the alloy interphase. Calculations suggest Mg thermodynamicaly prefers plating at the Mg|Mg-Ga interface rather than the Mg-Ga|electrolyte interface. Experimentally, Mg metal deposition on top of the interface is not observed by X-ray diffraction (XRD) or XPS and the interphase composition experiences minimal changes. However, kinetic limitations are present in the system, with the symmetric cell galvanostatic cycling at a relatively low current density of 0.1 mA cm^{-2} with a concentrated electrolyte (0.8 M Mg(TFSI)$_2$ in glyme) at moderately

*Electrochemical Society Member.
zE-mail: ksee@caltech.edu

elevated temperatures (40 °C). In addition, the Mg deposition underneath the interphase was not confirmed by cross-section SEM.[44] Meng et al. evaluated a Mg-Bi interphase, but its impact on Mg morphology was not discussed.[45]

Inspired by the initial work on alloy interphases, here we show an artificial interphase based on In metal and its alloys with Mg to reduce Mg dendrites and cell shorting. We then investigate the mechanism of the alloy interphase during reduction. The alloy-based interphase is prepared by a simple chemical redox reaction of Mg metal with $InBr_3$ in solution. The Mg-In interphase suppresses Mg dendrites, as observed by SEM. In a symmetric cell with glassy fiber separators, the Mg-In interphase results in a significant increase in the cycling lifetime before shorting. Ex-situ XRD shows the Mg content in the interphase increases as Mg^{2+} is reduced, indicating that magnesiation of the alloy phases occurs upon reduction instead of Mg metal plating. Cross-section SEM images show Mg deposition underneath the interphase, confirming Mg mobility through the interphase. Electrochemical characterization reveals that the electro-alloying of Mg into the Mg-In interphase is kinetically slow, resulting in a low threshold current density where exceeding said current density results in Mg deposition on top of the Mg-In interphase. The kinetic limitation is an important consideration to understand the behavior and benefits of the alloy interphase.

Experimental

General considerations.—All manipulations were performed in a N_2-filled glove box (MBraun, <1 ppm H_2O and O_2) unless otherwise stated. Tetrahydrofuran (THF, Fisher Scientific) was dried on a solvent purification system then dried over 4 Å sieves before use. Anhydrous $MgCl_2$ (99.9%, Fisher Scientific), anhydrous $AlCl_3$ (99.999%, Sigma Aldrich), anhydrous $InBr_3$ (99.99%, Thermo Scientific), and anhydrous hexanes (99%, mixed isomers, Sigma Aldrich) were used as received. Magnesium hexamethyldisilazide ($Mg(HMDS)_2$, 97%, Sigma Aldrich) was recrystallized in hexanes at −20 °C before use. Magnesium foil (99.9%, MTI Corporation, 0.1 mm thick) was cleaned with 0.1 M acetic acid in air, then brought inside the glove box, where it was further polished with 320 then 1500 grit silicon carbide sanding paper (3M).

Mg-In electrode and electrolyte preparation.—A 20 ml scintillation vial was charged with 17.8 mg of $InBr_3$, which was then dissolved in 5 ml of THF. The Mg foil was punched with a 6 mm hammer-driven punch or cut into appropriate pieces, then placed in the reaction vessel for *approx.* 2 h. The foil was then washed thoroughly in THF before use. The magnesium-aluminum chloride complex (MACC) electrolyte was prepared in an N_2-filled glove box according to Barile et al. with the addition of $Mg(HMDS)_2$ as in Kim et al. in 5 ml batches.[15,17] Solutions of $MACC+Mg(HMDS)_2$ (30 mM $AlCl_3$ + 60 mM $MgCl_2$ + 10 mM $Mg(HMDS)_2$) were prepared by adding 2.5 ml of chilled THF (cooled to approximately 0 °C on a Peltier plate) dropwise to anhydrous $AlCl_3$ (20 mg). THF (2.5 ml) was added to anyhdrous $MgCl_2$ (28.5 mg) and allowed to stir for 1 min. The $AlCl_3$ was completely dissolved in THF to yield a colorless solution. The $AlCl_3$ and $MgCl_2$ solutions were combined, and the resulting solution was stirred at 420 rpm until it turned clear and colorless (*approx.* 6 h). The electrolyte was subsequently conditioned by adding $Mg(HMDS)_2$ (17.5 mg) and allowed to stir until the solution turned clear.

Electrochemical measurements.—The galvanostatic cycling and long term deposition experiments were conducted on a VMP3 potentiostat (Bio-Logic) in a two-electrode geometry with the reference and the counter electrodes shorted. Cells were assembled in a 0.25 in inner diameter polytetrafluoroethylene (PTFE) Swagelok cells with Mo current collectors. GF/D (Whatman) filters were used as separators for the symmetric cell galvanostatic cycling experiments with 0.1 ml of $Mg(HMDS)_2$ electrolyte, at 0.025, 0.05, and 0.5 mA cm^{-2}, with 1 h half-cycles. The GF/D filters were punched

with a 0.25 in diameter hammer-driven punch and dried at 80 °C under reduced pressures before use. The long-term deposition experiments for ex-situ characterizations were done using a Mg|Mg-In working electrode and a Mg foil counter electrode. PTFE donut separator (0.25 in outer diameter, 0.125 in inner diameter) to eliminate scaffolding effects of a physical separator. The wells of the separator were filled with 0.05 ml of $MACC+Mg(HMDS)_2$ electrolyte.

Tandem deposition-cyclic voltammogram experiments for kinetics.—The experiments were concuted on a VMP3 potentiostat (Bio-Logic) in a three-electrode geometry. A Ag/Ag_2S reference was used,[46] which is well-characterized in the $MACC+Mg(HMDS)_2$ system.[47] Cells were assembled in a glass four-neck heart cell using electrode holders (Gamry Li BMC 1.5 mm substrate holder). The experiment consists of an initial deposition step for *approx.* 4 μAh cm^{-2}, then a 5 s open circuit hold, then a cyclic voltammetry (CV) scan from open circuit potential to −1 V then back to −1.7 V vs Ag/Ag_2S at 5 mV s^{-1}. This sequence is repeated for different current densities, at 0.01, 0.025, 0.05, 0.075, 0.1, and 0.5 mA cm^{-2}.

Physical characterizations.—All characterization was completed on working electrodes after rinsing with 1 ml of THF and drying in a N_2 glove box. SEM images were taken with a ZEISS 1150 variable pressure field emission scanning electron microscope with a 15 kV accelerating voltage and an in-lens secondary electron detector. Energy dispersive X-ray spectroscopy (EDS) data were collected using an Oxford X-Max Silicon Drift Detectors X-ray energy dispersive spectrometer with a 15 kV accelerating voltage. Samples were briefly exposed to air during transfer into the instrument. Cross sections of electrode samples were taken by cooling the electrode with liquid nitrogen, then cutting with a scalpel. XRD patterns of the Mg-In electrodes were collected using the Rigaku SmartLab diffractometer equipped with a HyPix-3000 detector and a Cu Kα X-ray source with a 40 kV accelerating voltage, using a Rigaku airtight sample holder. The patterns were collected from 10 to 50° 2θ at 3° per minute in a Bragg-Brentano geometry. The grazing incidence XRD pattern of the pristine Mg|Mg-In electrode was collected in a parallel beam geometry with an ω of 0.3°.

Results and Discussion

First we discuss the preparation of the Mg-In alloy interphase. The modified electrode is prepared by a chemical reaction of Mg metal with 50 mM $InBr_3$ in tetrahydrofuran (THF). Mg is a stronger reducing agent compared to In with an E^0 of −2.36 V vs the standard hydrogen electrode (SHE)[48] compared to −0.34 V[49] vs SHE for In. The Mg metal can therefore chemically reduce the In^{3+} in solution. To determine the fate of the Br^-, EDS is measured on the Mg metal surface after reaction (Fig. S3). Negligible quantities of Br are detected in the interphase via EDS (roughly estimated at <1% by weight), which suggests the $MgBr_2$ precipitates out into solution rather than on the interface. After reaction with $InBr_3$, the foil turns gray. If the foil is allowed to react for a longer period, on the order of 20 h, then the surface layer flakes off revealing reactive Mg metal. Thus, the reaction is not self-limiting. To evaluate the morphology of the solid reaction product on the Mg surface, SEM images are taken of the Mg metal surface before and after a 2 h reaction with $InBr_3$. The SEM images is shown in Figs. 1a, 1b. The Mg foil before the reaction with $InBr_3$ is smooth with some grooves from the polishing process with sandpaper. After the reaction, the surface layer is rough and uneven, but covers the entire exposed Mg surface.

The XRD pattern measured in Bragg-Brentano geometry of the Mg foil after the reaction with $InBr_3$ is shown in Fig. 1c. The (002) reflection of Mg metal is the strongest peak, suggesting that the X-rays can penetrate through the surface film to the Mg metal substrate (Fig. S1). However, additional peaks are observed suggesting the surface layer has crystalline domains. The additional
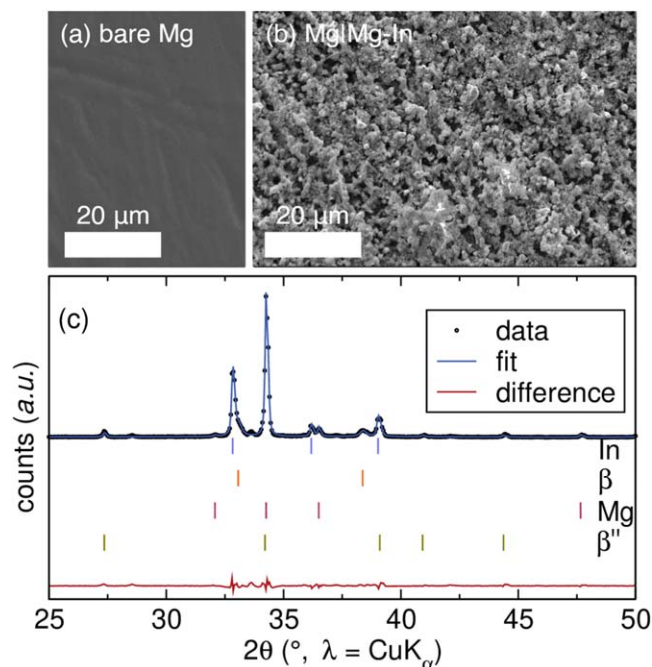
Figure 1. SEM image of the Mg metal foil (a) before and (b) after reaction with InBr$_3$ in THF for 2 h. A rough surface film is observed after reaction across the foil. (c) XRD pattern of the Mg foil after reaction with InBr$_3$ with a four phase Rietveld refinement to Mg, In, and the Mg-In alloys β and β'', collected in a Bragg-Brentano geometry.

Figure 2. Galvanostatic cycling of Mg metal and Mg|Mg-In electrodes at (a) 0.025 mA cm^{-2} and (b) 0.5 mA cm^{-2} using MACC + Mg(HMDS)$_2$ electrolyte with a glassy fiber separator. Each half-cycle is 1 h. A higher overpotential and faster shorting behavior is observed with bare Mg metal electrodes when compared to Mg|Mg-In electrodes at low current densities. When cycling at 0.5 mA cm^{-2}, there are no meaningful differences between the galvanostatic behavior of bare Mg and Mg|Mg-In electrodes.

peaks can be assigned via a four phase Rietveld refinement to In metal and two different Mg-In compounds in the binary phase space: β and β''.[50] The β phase is a disordered *fcc* structure that forms at high In content at lower temperatures, and <50% In content at higher temperatures.[51] The β'' phase is an ordered tetragonal structure that forms near 50% In content. The β'' phase forms upon slow cooling between In contents of 35 to 50%, suggesting the phase is thermodynamically favorable at the specified In contents.[52] Both the alloys have a moderately wide solid-solubility window near room temperature (*approx.* 10% in composition), which may enable the electroalloying of Mg upon reduction. Both In and Mg metals have some degree of solubility as well. From the quality of the diffraction pattern collected, we were unable to determine the exact Mg-In contents within each phase. We can estimate the phase fractions of each crystalline phase within the Mg-In interphase from the Rietveld refinement by excluding the Mg fraction due to the visible contributions from the Mg foil substrate. The phase fractions of the phases given in weight percent are 62% In, 15% β'', and 23% β. Because multiple phases are formed after reaction with InBr$_3$, we will refer to the surface film as the Mg-In interphase hereafter. Mg foil electrodes with the Mg-In interphase will be referred to as Mg|Mg-In electrodes.

To investigate the effects of the Mg-In interphase on the electrochemical stripping and deposition of Mg^{2+}, the Mg|Mg-In electrode is galvanostatically cycled in a symmetric cell and compared to a bare Mg control. The galvanostatic cycling data are shown in Fig. 2. The electrolyte of choice for the electrochemical characterization of the electrode is a MACC electrolyte chemically conditioned with Mg(HMDS)$_2$.[53] MACC + Mg(HMDS)$_2$ is chosen for its high anodic stability compared to Grignard-based electrolytes and its potential susceptibility for dendrites due to its low Mg^{2+} concentration (60 mM) that causes low conductivity. A PTFE Swagelok union cell with Mo current collectors are used to avoid stainless steel corrosion with the chloride-containing electrolyte. At a current density of 0.025 mA cm^{-2}, bare Mg metal electrodes show a rapid increase in the plating and stripping overpotential until erratic spikes are observed after about 9 cycles, which is attributed to
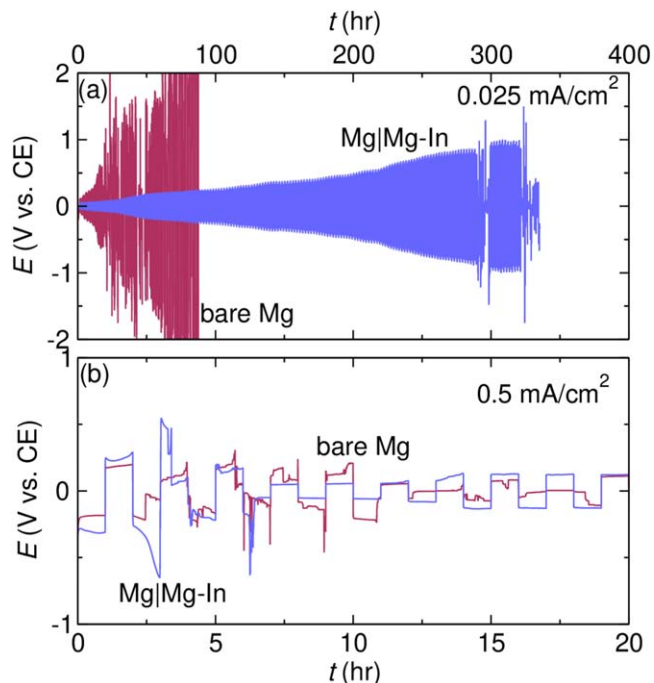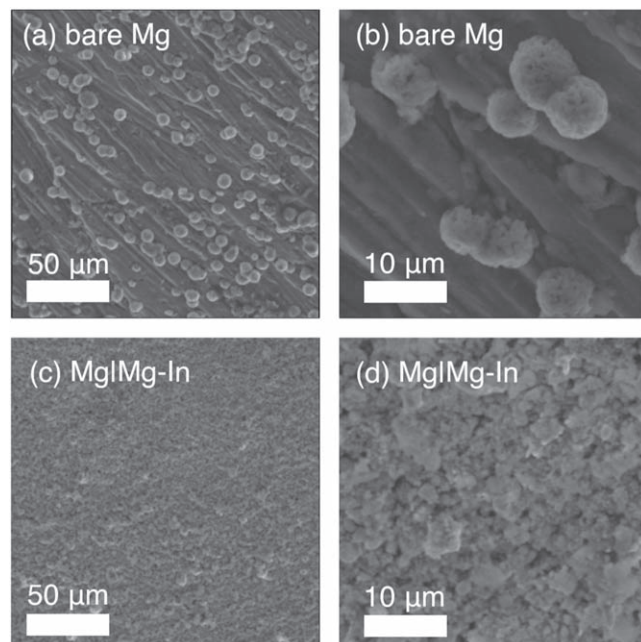

Figure 3. SEM images of the (a), (b) bare Mg and (c), (d) Mg|Mg-In electrode after applying −0.05 mA cm^{-2} for 10 h. A PTFE donut separator is used to prevent the separator from affecting the morphology. A heterogeneous deposit is clearly observed in (a), (b) while absent in (c), (d).

electrical soft shorts in the cell (Fig. 2a). Upon disassembly of the cell, black deposits are observed on both sides of the porous glassy fiber separator which we assume to be Mg. In contrast, the Mg|Mg-In electrodes exhibit a much slower and gradual increase in overpotential, and cell shorting is not observed until after 144 cycles
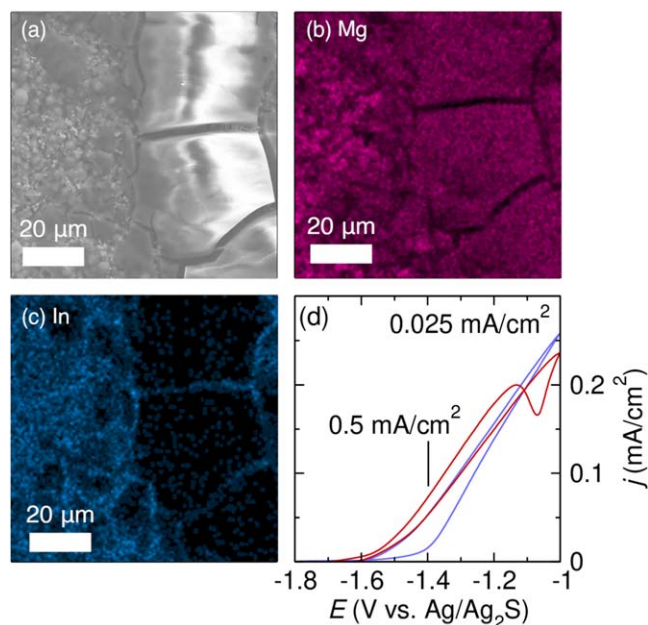
Figure 4. (a) SEM image, (b) Mg EDS map, and (c) In EDS map of the Mg|Mg-In electrode after a deposition of 1.25 mAh cm^{-2} at a current density of 0.5 mA cm^{-2}. Large Mg deposits are observed on the surface. (d) Cyclic voltammograms of the Mg|Mg-In electrode swept at 5 mV s^{-1} after a deposition of 3 mC, at a current density of either 0.025 mA cm^{-2} or 0.5 mA cm^{-2}. The small anodic peak observed after higher current density deposition is an indicator of Mg deposits on top of the Mg|Mg-In electrode.

(Fig. 2a). The increasing overpotentials upon galvanostatic cycling suggests an instability in the Mg|Mg-In electrode upon extended cycling, likely the result of an insulating interphase forming on top of the Mg-In alloy, or a mechanical breakdown of the Mg-In alloy. However, compared to galvanostatic cycling results of bare Mg electrodes, the overpotential increase is much slower, suggesting an improvement in the electrode stability. The galvanostatic cycling behavior at 0.05 mA cm^{-2} is shown in Fig. S4, and similar trends hold. However, 0.05 mA cm^{-2} is not a commercially relevant current density. As such, the symmetric cells were cycled at elevated current densities to study the kinetic limitations of the Mg|Mg-In electrodes. The galvanostatic cycling performance of the bare Mg and Mg|Mg-In electrodes at a current density of 0.5 mA cm^{-2} are shown in Fig. 2b. No meaningful differences in electrochemical performance between bare Mg and the Mg|Mg-In electrode are observed, suggesting a possible kinetic limitation with the interphase.

First, we probe the low current reduction behavior to investigate the changes to morphology. SEM images of the electrode surfaces are taken after applying −0.05 mA cm^{-2} for 10 h. To eliminate the effect of the separator scaffolding on the deposition morphology, a donut PTFE separator is used in a Swagelok cell. The well of the separator is filled with the electrolyte solution, thus providing a planar electrode surface with no scaffolding to seed nucleation or affect growth morphology. The SEM image of the bare Mg electrode after reduction is shown in Figs. 3a and 3b. Small spherical Mg clusters are found scattered across the electrode. This morphology is similar to the Mg deposits observed by Eaves-Rathert and coworkers, arising from hemispherical deposition of Mg under moderate overpotentials.[33] The SEM of the Mg|Mg-In electrode after reduction is shown in Figs. 3c and 3d. In contrast to the bare Mg electrode, the Mg|Mg-In electrode morphology changes minimally with the rough surface becoming marginally less fractal. No hemispherical growths are observed suggesting Mg is not plated on the surface. To determine if the Mg-In alloy remains intact following an oxidation, the Mg|Mg-In electrode is oxidized at 0.05 mA cm^{-2} and imaged. The SEM and corresponding EDS maps are found in the SI in

Fig. S18. In is still present homogenously dispersed on the electrode surface following oxidation, suggesting that at least for short term cycling, the Mg-In alloy remains intact.

However, the significantly different galvanostatic cycling behavior of the Mg|Mg-In electrode at a higher current density suggests different processes are occuring at high current densities. To study the surface morphology after a high current reduction step, SEM images of the Mg|Mg-In electrode surface after a reduction at −0.5 mA cm^{-2} are collected. The SEM image and the EDS elemental maps of the Mg|Mg-In electrode surface after the reduction are shown in Figs. 4a–4c. Contrary to the morphology at low current density, deposits are observed on top of the electrode with no In present in the deposits, indicating the deposits are Mg metal. Thus, there appears to be a rate at which Mg will deposit on top of the interphase.

To electrochemically probe if Mg is deposited at the electrode surface, i.e. on top of the Mg-In surface, a two-stage electrochemical experiment is devised. First, the Mg|Mg-In electrode is reduced at a constant current density. Then, a positive sweep cyclic voltammogram (CV) is collected. The experiment is repeated with increasing current densities. Two CVs from the experiment are presented in Fig. 4d, one after a deposition at 0.025 mA cm^{-2} and another at 0.5 mA cm^{-2}. The CV after reduction at 0.5 mA cm^{-2} exhibits a depletion effect where the current density decreases as the potential is swept positively. This depletion effect in the CV is attributed to stripping of freshly-deposited surface Mg on top of the Mg-In interphase, such as the deposit imaged in Fig. 4a. Once all the freshly-deposited Mg is stripped off, the current density decreases. A similar phenomenon was observed by Melemed et al. where a depletion effect was observed via CVs after a deposition of fresh Ca on top of a passivation layer.[54] However, no such depletion effect is observed in the CV after reduction at 0.025 mA cm^{-2}, which indicates no such deposited Mg is available on the surface of the electrode. A clear kinetic limitation in the Mg-In interphase is therefore observed where past a critical current density, the Mg-In interphase acts as a deposition substrate instead of suppressing dendrites.

To gain more insights into the reduction process in the Mg|Mg-In electrode, we investigate the mechanism by characterizing the Mg|Mg-In electrode after reduction ex-situ. First, the XRD pattern of the Mg|Mg-In electrodes are collected after reduction at low current densities to observe the changes in the crystalline domains in the interphase. In Fig. 5, the XRD patterns of the Mg|Mg-In electrode before and after reduction are shown. The patterns can be fit via a Rietveld refinement to the four phases identified in Fig. 1c: Mg, In, and the binary Mg-In alloys β and β''. The largest peak is the Mg(002) reflection with a preferential orientation for the (002) plane, which suggest that the X-rays penetrate through the entire Mg-In interphase to the Mg foil substrate. Therefore, we assume that all the crystalline phases of the Mg-In interphase are captured by XRD. All the In-containing phases can be fit well due to isolated peaks. The intensities of the two XRD patterns are normalized to the Mg(101) reflection to better compare the relative intensities of the reflections of different phases. After reduction of the Mg|Mg-In electrode, an increase in the intensity of the reflections attributed to the β'' phase is observed. The increase in intensity is most evident in the β''(100) reflection near 27° 2θ. A corresponding decrease in the intensity in the In reflections is observed, easily observable in the In(101) and In(002) reflections near 33° 2θ and 36° 2θ, respectively. The calculated phase fractions from the Rietveld refinement are shown in Table I. Upon reduction of the Mg|Mg-In electrode, a clear decrease in the In phase fraction is observed, as well as a slight decrease in the In-rich β phase alloy. A significant increase in the Mg-rich β'' phase is observed. The XRD patterns thusly indicate that the crystalline domains of the Mg-In interphase magnesiates upon reduction. Based on the diffraction patterns, two possible mechanisms can be posed. The Mg-In alloy could act essentially as an alloy electrode deposited on a conductive substrate (Mg), where the redox occurs only on the deposited alloys.
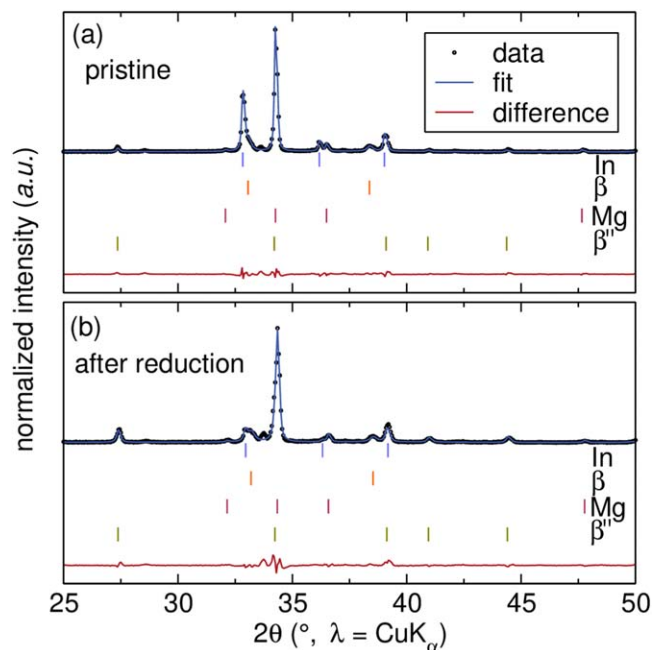
Figure 5. XRD patterns of the Mg|Mg-In electrode in a (a) pristine condition and (b) after a 0.025 mA cm^{-2} reduction for 100 h. The patterns are fit with a four-phase Rietveld refinement that includes In, Mg, and two Mg-In phases β and β''. Upon reduction, a growth of the Mg-rich β'' phase is observed with a corresponding decrease in In metal.

Table I. Phase fractions of the In-related phases present in the interphase layer, as calculated from the Rietveld refinement.

Phases[a]	Pristine (wt%)	Reduced (wt%)
In	62%	16%
β''	15%	64%
β	23%	20%

a) The Mg phase is excluded as the X-ray penetrates through the alloy layer into the Mg substrate. The remaining three phases are renormalized.

Indeed, In and the β'' phase alloy have been shown in literature to be capable of acting as Mg bulk alloy electrodes with changing Mg contents as the electrode reduces and oxidizes.[55] A similar phenomenon is observed in the Mg-Hg amalgam surface system, where upon reduction of the surface modified electrode, an increase in magnesiation in the Mg-Hg alloy on the surface of the electrode is observed. Based on the increase in magnesiation upon reduction in the alloy interphase, the authors suggest that the amalgam surface is not active as a protective surface, but rather as a simple Mg-Hg alloy electrode deposited on top of an inert Mg metal substrate.[56] However, an alternate mechanism can be hypothesized, wherein Mg mobility through the interphase can occur alongside alloying into the interphase, allowing Mg to plate underneath the interphase.

To determine whether Mg mobility through the Mg-In interphase is possible, ex-situ cross-section SEM images of the Mg|Mg-In electrodes before and after reduction are collected. The cross-section SEM image of the Mg|Mg-In electrode before reduction with the corresponding EDS map is shown in Figs. 6a–6d. The EDS map shows a mix of both Mg and In in the interphase layer, which is *approx.* 5 μm thick. Some O is found on the surface layer, likely due to air exposure during sample preparation and transfer.

The cross-section SEM image of the Mg|Mg-In electrode after reduction is shown in Figs. 6e–6h. Mg deposits of a different morphology from the Mg foil substrate are observed beneath the Mg-In interphase. Interestingly, the deposits do not form a uniform layer underneath, instead forming localized veins. We hypothesize that Mg nucleation occurs preferentially underneath the interphase where the interphase is the thinnest, due to the kinetic limitations of the interphase. Upon nucleation, further Mg deposition preferentially occurs at these sites. The deposited Mg also exhibits more oxidation during sample preparation compared to the Mg substrate as evidenced by the O EDS map (Figs. 6d and 6h). The increased surface area of the deposited Mg compared to the densely packed
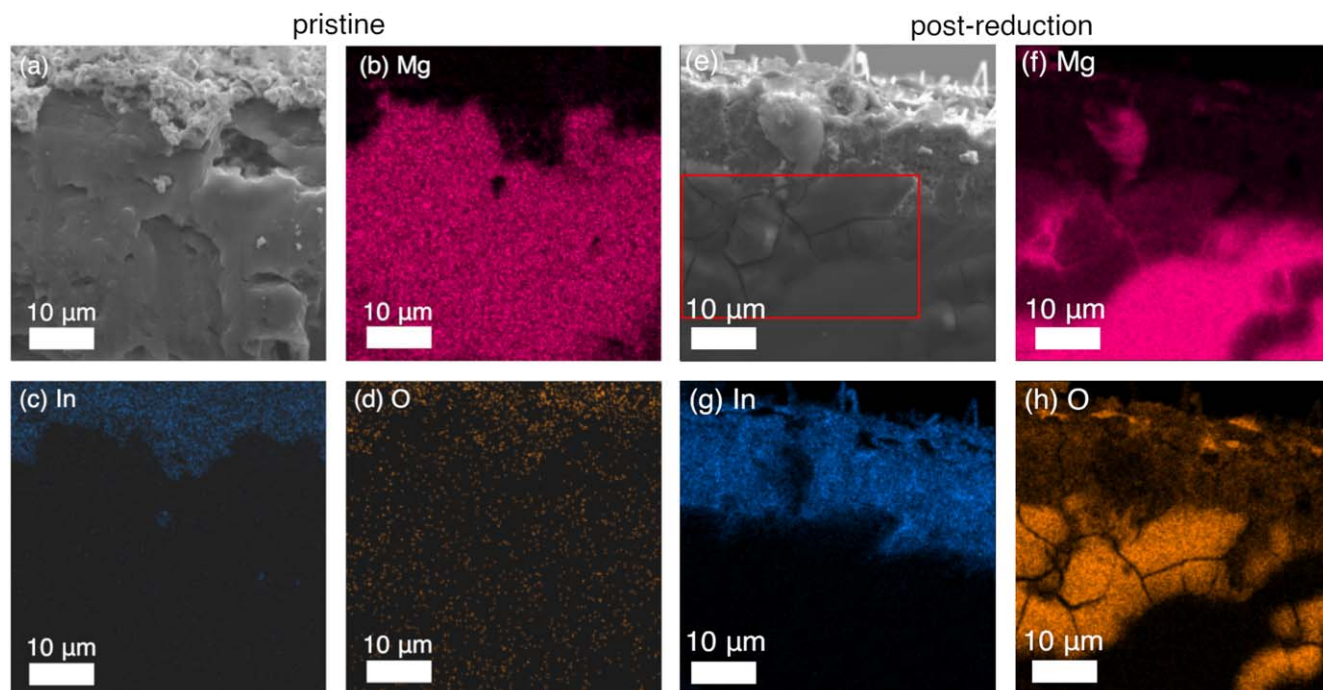

Figure 6. (a) Cross-section SEM image of the pristine Mg|Mg-In electrodes and corresponding EDS maps for (b) Mg, (c) In, and (d) O. (e) Cross-section SEM images of the Mg|Mg-In electrode after a 100 hrdeposition at 0.025 mA cm^{-2} and corresponding EDS maps for (f) Mg, (g) In, and (h) O. Compared to the pristine Mg|Mg-In electrode, the Mg underneath the Mg-In layer is clearly heterogeneous, with freshly deposited veins of Mg visible in the Mg and O maps.
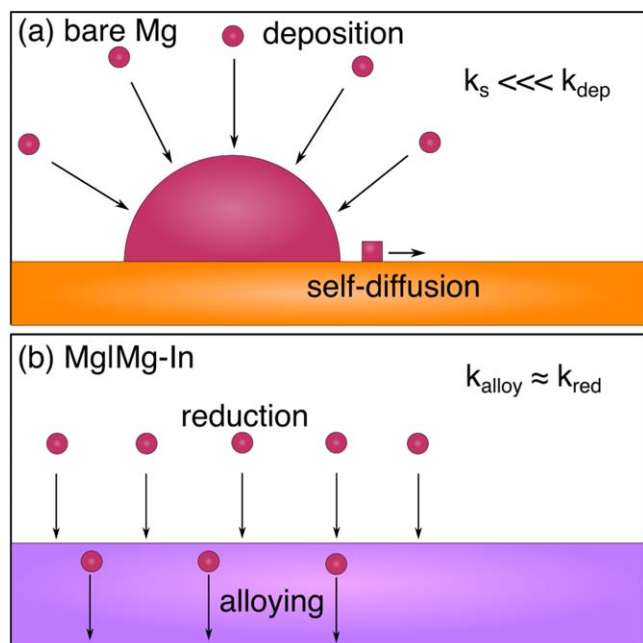
Figure 7. Cartoon illustrations of the Mg^{2+} reduction process at (a) bare Mg and (b) Mg|Mg-In electrode surfaces. In bare Mg, the rate of self-diffusion (k_s) of Mg across the surface is in competition with the rate of deposition (k_{dep}), while in Mg|Mg-In electrodes, the rate of alloying (k_{alloy}) competes against the rate of reduction (k_{red}) to determine the morphology.

commercial Mg foil likely causes faster oxidation in the deposited Mg. Some Mg deposits are also observed on top of the interphase, which is attributed to the depletion effects associated with the extreme length of the reduction necessary to deposit enough Mg underneath the interphase to observe with an SEM (100 h rat 0.025 mA cm^{-2}) (Fig. S17). No Mg deposits are observed when a shorter reduction time was used, as seen above in Figs. 3c–3d.

Discussion

Next we discuss the results in the context of metal deposition models. Chazalviel and coworkers described a model in which the dendritic growth of metals is caused by the formation of a space charge region at the surface of the cathode, due to repulsion of anions and consumption of cations.[29,57] The model is used to describe the diffusion-limited aggregation (DLA) that causes the classic branching dendritic morphology. However, the deposits observed in Figs. 3a and 3b do not resemble a DLA morphology. Instead, the deposits observed on a bare Mg electrode are better described as hemispherical growth. Hemispherical growth occurs under mixed diffusion and kinetic control at intermediate current densities. Unlike a DLA regime, full mass transport limitation is not yet achieved.[58] A cartoon of the reduction process with a bare Mg electrode is shown in Fig. 7a. The kinetics of the deposition overtake the kinetics of the self-diffusion of Mg across the surface. As such, instead of forming a smooth surface and minimizing the surface energy, the cations reduce as soon as they arrive on the surface.

Based on our experimental observations, we theorize that the electroreduction process at the Mg|Mg-In electrode is different. Processes occurring on the Mg|Mg-In electrode are governed by different rates. In Fig. 7b, the same reduction process is shown instead with an alloy interphase. In the Mg|Mg-In electrode, upon reduction of the Mg^{2+} cation at the surface of the electrode, the cation alloys into the Mg-In interphase. The alloying process appears more facile than the self-diffusion of Mg, indicated by the suppression of dendrites at same current densities. As such, even at moderate current densities, the alloying process can kinetically keep up with the cation flux. The concentration gradient in the interphase then causes Mg to diffuse, depositing underneath the interphase at the Mg|Mg-In interface. At elevated current densities however, the diffusion through the Mg-In interphase becomes kinetically limiting, resulting in Mg deposition on top of the interphase.

The kinetic limitation of the alloy interphase controlling the deposition location of the metal is also observed in literature in Li alloy interphase systems. In a Li-Sn interphase system, Li plates underneath the interphase below the exchange current density of the Li|Li-Sn electrode. However, upon increasing the deposition current density past the exchange current density, Li begins plating on top of the Li-Sn interphase.[59] In another study investigating a Li-Sn interphase system, computed surface energies of the electrode surface suggest that at low current densities, plating underneath the interphase is energetically favorable, but at high current densities Li accumulates at the surface and delaminates.[60]

Conclusions

Herein, we demonstrate more uniform reduction with a Mg electrode with a Mg-In alloy interphase compared to Mg metal. The Mg|Mg-In electrode is easily prepared by a chemical reaction of a Mg foil with a solution of InBr$_3$ in THF. The Mg|Mg-In electrode is capable of undergoing more deposition and stripping cycles before evidence of soft shorts are observed compared to Mg metal. While Mg electrodes grow heterogeneous Mg deposits upon reduction, the Mg|Mg-In electrodes do not under the same conditions and instead undergo alloying reactions followed by Mg deposition occurring below the alloy. However, the Mg|Mg-In electrode is kinetically limited by the alloying process. At higher current densities, the alloying kinetics cannot keep up with the rate of Mg^{2+} reduction and Mg deposits on top of the Mg-In interphase. Improved alloy interphases thus must have higher Mg mobility, again highlighting the crucial role of divalent solid-state ion conductivity in Mg-based electrochemical cells. Higher mobility could be achieved by targeting a new phase or leveraging defect engineering strategies. Nevertheless, the Mg-In system serves as a proof-of-concept system for the use of alloy interphases to leverage alloy solid solubility to reduce Mg deposition and cell shorting, an issue that is likely to impact commercial cells due to the use of separators.

ORCID

Brian C. Lee https://orcid.org/0000-0002-0898-0838
Kimberly A. See https://orcid.org/0000-0002-0133-9693

References

1. U.S. Geological Survey, Mineral Commodity Summaries 2019; 2019.
2. E. Peled and H. Straze, "The kinetics of the magnesium electrode in thionyl chloride solutions." *J. Electrochem. Soc.*, **124**, 1030 (1977).
3. L. P. Lossius and F. Emmenegger, "Plating of magnesium from organic solvents." *Electrochim. Acta*, **41**, 445 (1996).
4. C. Liebenow, "Reversibility of electrochemical magnesium deposition from grignard solutions." *J. Appl. Electrochem.*, **27**, 221 (1997).
5. Z. Lu, A. Schechter, M. Moshkovich, and D. Aurbach, "On the electrochemical behavior of magnesium electrodes in polar aprotic electrolyte solutions." *J. Electroanal. Chem.*, **466**, 203 (1999).
6. J. G. Connell, B. Genorio, P. P. Lopes, D. Strmcnik, V. R. Stamenkovic, and N. M. Markovic, "Tuning the reversibility of mg anodes via controlled surface passivation by h2o/cl–in organic electrolytes." *Chem. Mater.*, **28**, 8268 (2016).

7. L. W. Gaddum and H. E. French, "The electrolysis of grignard solutions." *J. Am. Chem. Soc.*, **49**, 1295 (1927).

8. W. V. Evans and R. Pearson, "The ionic nature of the grignard reagent." *J. Am. Chem. Soc.*, **64**, 2865 (1942).

9. J. D. Genders and D. Pletcher, "Studies using microelectrodes of the mg(ii)/mg couple in tetrahydrofuran and propylene carbonate." *J. Electroanal. Chem. Interfac. Electrochem.*, **199**, 93 (1986).

10. D. Aurbach, H. Gizbar, A. Schechter, O. Chusid, H. E. Gottlieb, Y. Gofer, and I. Goldberg, "Electrolyte solutions for rechargeable magnesium batteries based on organomagnesium chloroaluminate complexes." *J. Electrochem. Soc.*, **149**, A115 (2002).

11. O. Mizrahi, N. Amir, E. Pollak, O. Chusid, V. Marks, H. Gottlieb, L. Larush, E. Zinigrad, and D. Aurbach, "Electrolyte solutions with a wide electrochemical window for rechargeable magnesium batteries." *J. Electrochem. Soc.*, **155**, A103 (2007).

12. Y. Vestfried, O. Chusid, Y. Goffer, P. Aped, and D. Aurbach, "Structural analysis of electrolyte solutions comprising magnesium-aluminate chloro-organic complexes by raman spectroscopy." *Organometallics*, **26**, 3130 (2007).

13. R. E. Doe, R. Han, J. Hwang, A. J. Gmitter, I. Shterenberg, H. D. Yoo, N. Pour, and D. Aurbach, "Novel electrolyte solutions comprising fully inorganic salts with high anodic stability for rechargeable magnesium batteries." *Chem. Commun.*, **50**, 243 (2014).

14. T. Liu, Y. Shao, G. Li, M. Gu, J. Hu, S. Xu, Z. Nie, X. Chen, C. Wang, and J. Liu, "A facile approach using mgcl 2 to formulate high performance Mg 2. electrolytes for rechargeable mg batteries." *J. Mater. Chem. A*, **2**, 3430 (2014).

15. C. J. Barile, E. C. Barile, K. R. Zavadil, R. G. Nuzzo, and A. A. Gewirth, "Electrolytic conditioning of a magnesium aluminum chloride complex for reversible magnesium deposition." *J. Phys. Chem. C*, **118**, 27623 (2014).

16. J. H. Ha, B. Adams, J.-H. Cho, V. Duffort, J. H. Kim, K. Y. Chung, B. W. Cho, F. L. Nazar, and S. H. Oh, "A conditioning-free magnesium chloride complex electrolyte for rechargeable magnesium batteries." *J. Mater. Chem. A*, **4**, 7160 (2016).

17. S. S. Kim, S. C. Bevilacqua, and K. A. See, "Conditioning-free mg electrolyte by the minor addition of Mg(HMDS)2." *ACS Appl. Mater. Interfaces*, **12**, 5226 (2020).

18. D.-T. Nguyen, A. Y. S. Eng, M.-F. Ng, V. Kumar, Z. Sofer, A. D. Handoko, G. S. Subramanian, and Z. W. Seh, "A high-performance magnesium triflate-based electrolyte for rechargeable magnesium batteries." *Cell Rep. Phys. Sci.*, **1**, 100265 (2020).

19. S.-Y. Ha, Y.-W. Lee, S. W. Woo, B. Koo, J.-S. Kim, J. Cho, K. T. Lee, and N.-S. Choi, "Magnesium(II) bis(trifluoromethane sulfonyl) imide-based electrolytes with wide electrochemical windows for rechargeable magnesium batteries." *ACS Appl. Mater. Interfaces*, **6**, 4063 (2014).

20. I. Shterenberg, M. Salama, H. D. Yoo, Y. Gofer, J.-B. Park, Y.-K. Sun, and D. Aurbach, "Evaluation of (CF3SO2)2N- (TFSI) based electrolyte solutions for Mg batteries." *J. Electrochem. Soc.*, **162**, A7118 (2015).

21. M. Salama et al., "Unique behavior of dimethoxyethane (DME)/Mg(N(SO2CF3)2) 2 solutions." *J. Phys. Chem. C*, **120**, 19586 (2016).

22. J. T. Herb, C. A. Nist-Lund, and C. B. Arnold, "A fluorinated alkoxyaluminate electrolyte for magnesium-ion batteries." *ACS Energy Lett.*, **1**, 1227 (2016).

23. Z. Zhao-Karger, M. E. G. Bardaji, O. Fuhr, and M. Fichtner, "A new class of non-corrosive, highly efficient electrolytes for rechargeable magnesium batteries." *J. Mater. Chem. A*, **5**, 10815 (2017).

24. R. Mohtadi, M. Matsui, T. S. Arthur, and S.-J. Hwang, "Magnesium borohydride: from hydrogen storage to magnesium battery." *Angew. Chem. Int. Ed.*, **51**, 9780 (2012).

25. T. J. Carter, R. Mohtadi, T. S. Arthur, F. Mizuno, R. Zhang, S. Shirai, and J. W. Kampf, "Boron clusters as highly stable magnesium-battery electrolytes." *Angew. Chem. Int. Ed.*, **53**, 3173 (2014).

26. M. Matsui, "Study on electrochemically deposited Mg metal." *J. Power Sources*, **196**, 7048 (2011).

27. M. Jäckle and A. Groß, "Microscopic properties of lithium, sodium, and magnesium battery anode materials related to possible dendrite growth." *J. Chem. Phys.*, **141**, 174710 (2014).

28. C. Hendricks, N. Williard, S. Mathew, and M. Pecht, "A failure modes, mechanisms, and effects analysis (fmmea) of lithium-ion batteries." *J. Power Sources*, **297**, 113 (2015).

29. J.-N. Chazalviel, "Electrochemical aspects of the generation of ramified metallic electrodeposits." *Phys. Rev. A*, **42**, 7355 (1990).

30. V. Fleury, M. Rosso, J.-N. Chazalviel, and B. Sapoval, "Experimental aspects of dense morphology in copper electrodeposition." *Phys. Rev. A*, **44**, 6693 (1991).

31. R. M. Brady and R. C. Ball, "Fractal growth of copper electrodeposits." *Nature*, **309**, 225 (1984).

32. R. Davidson et al., "Formation of magnesium dendrites during electrodeposition." *ACS Energy Lett.*, **4**, 375 (2019).

33. J. Eaves-Rathert, K. Moyer, M. Zohair, and C. L. Pint, "Kinetic- versus diffusion-driven three-dimensional growth in magnesium metal battery anodes." *Joule*, **4**, 1324 (2020).

34. S. Hebié, H. P. K. Ngo, J.-C. Leprêtre, C. Iojoiu, L. Cointeaux, R. Berthelot, and F. Alloin, "Electrolyte based on easily synthesized, low cost triphenolate--borohydride salt for high performance Mg(TFSI)2 rechargeable magnesium batteries." *ACS Appl. Mater. Interfaces*, **9**, 28377 (2017).

35. S. Hebié, F. Alloin, C. Iojoiu, R. Berthelot, and J.-C. Leprêtre, "Magnesium anthracene system-based electrolyte as a promoter of high electrochemical performance rechargeable magnesium batteries." *ACS Appl. Mater. Interfaces*, **10**, 5527 (2018).

36. M. S. Ding, T. Diemant, R. J. Behm, S. Passerini, and G. A. Giffin, "Dendrite growth in Mg metal cells containing Mg(TFSI)2/glyme electrolytes." *J. Electrochem. Soc.*, **165**, A1983 (2018).

37. S.-B. Son, T. Gao, S. P. Harvey, K. X. Steirer, A. Stokes, A. Norman, C. Wang, A. Cresce, K. Xu, and C. Ban, "An artificial interphase enables reversible magnesium chemistry in carbonate electrolytes." *Nat. Chem.*, **10**, 532 (2018).

38. Z. Liang and C. Ban, "Strategies to enable reversible magnesium electrochemistry: from electrolytes to artificial solid–electrolyte interphases." *Angew. Chem. Int. Ed.*, **60**, 11036 (2021).

39. Y. Zhao, A. Du, S. Dong, F. Jiang, Z. Guo, X. Ge, X. Qu, X. Zhou, and G. Cui, "A bismuth-based protective layer for magnesium metal anode in noncorrosive electrolytes." *ACS Energy Lett.*, **6**, 2594 (2021).

40. S. Shin, J. H. Kwak, S. H. Oh, H.-S. Kim, S.-H. Yu, and H.-D. Lim, "Reversible Mg-metal batteries enabled by a Ga-rich protective layer through one-step interface engineering." *ACS Appl. Mater. Interfaces*, **15**, 28684 (2023).

41. B. Yang, L. Xia, R. Li, G. Huang, S. Tan, Z. Wang, B. Qu, J. Wang, and F. Pan, "Superior plating/stripping performance through constructing an artificial interphase layer on metallic Mg anode." *J. Mat. Sci. Technol.*, **157**, 154 (2023).

42. B. Wan, B. Dou, X. Zhao, J. Wang, W. Zhao, M. Guo, Y. Zhang, J. Li, Z.-F. Ma, and X. Yang, "Three-dimensional magnesiophilic scaffolds for reduced passivation toward high-rate mg metal anodes in a noncorrosive electrolyte." *ACS Appl. Mater. Interfaces*, **12**, 28298 (2020).

43. R. Lv, X. Guan, J. Zhang, Y. Xia, and J. Luo, "Enabling Mg metal anodes rechargeable in conventional electrolytes by fast ionic transport interphase." *Natl. Sci. Rev.*, **7**, 333 (2020).

44. C. Pechberty et al., "Alloying electrode coatings towards better magnesium batteries." *J. Mater. Chem. A*, **10**, 12104 (2022).

45. Z. Meng, Z. Li, L. Wang, T. Diemant, D. Bosubabu, Y. Tang, R. Berthelot, Z. Zhao-Karger, and M. Fichtner, "Surface engineering of a mg electrode via a new additive to reduce overpotential." *ACS Appl. Mater. Interfaces*, **13**, 37044 (2021).

46. C. Horwood and M. Stadermann, "Evaluation of a Ag/Ag2S reference electrode with long-term stability for electrochemistry in ionic liquids." *Electrochem. Commun.*, **88**, 105 (2018).

47. F. A. L. Laskowski, S. H. Stradley, M. D. Qian, and K. A. See, "Mg anode passivation caused by the reaction of dissolved sulfur in Mg–S batteries." *ACS Appl. Mater. Interfaces*, **13**, 29461 (2021).

48. A. J. Bard and L. R. Faulkner, *Electrochemical Methods* (John Wiley & Sons) 2nd ed. (2001).

49. A. J. Bard, R. Parsons, and J. Jordan, *Standard Potentials in Aqueous Solution* (CRC Press, New York City, NY) 1st ed. (1985).

50. A. A. Nayeb-Hashemi and J. B. Clark, "The In-Mg (indium-magnesium) system." *Bull. Alloy Phase Diag.*, **6**, 149 (1985).

51. G. V. Raynor, "The constitution of the magnesium-indium alloys in the region 20 to 50 atomic per cent of indium." *Trans. Faraday Soc.*, **44**, 15 (1948).

52. K. Schubert, F. Gauzzi, and K. Frank, "Kristallstruktur einiger Mg-B3-Phasen." *Z. Metallkde.*, **54**, 422 (1963).

53. H. S. Kim, T. S. Arthur, G. D. Allred, J. Zajicek, J. G. Newman, A. E. Rodnyansky, A. G. Oliver, W. C. Boggess, and J. Muldoon, "Structure and compatibility of a magnesium electrolyte with a sulphur cathode." *Nat. Commun.*, **2**, 427 (2011).

54. A. M. Melemed and B. M. Gallant, "Electrochemical signatures of interface-dominated behavior in the testing of calcium foil anodes." *J. Electrochem. Soc.*, **167**, 140543 (2020).

55. F. Murgia, E. T. Weldekidan, L. Stievano, L. Monconduit, and R. Berthelot, "First investigation of indium-based electrode in mg battery." *Electrochem. Commun.*, **60**, 56 (2015).

56. C. Pechberty, J.-B. Ledeuil, J. Allouche, R. Dedryvère, L. Stievano, and R. Berthelot, "Surface amalgam on magnesium electrode: protective coating or not?" *Energy Technol.*, **11**, 2201098 (2023).

57. V. Fleury, J. N. Chazalviel, M. Rosso, and B. Sapoval, "The role of the anions in the growth speed of fractal electrodeposits." *J. Electroanal. Chem. Interfacial Electrochem.*, **290**, 249 (1990).

58. L. Guo and P. C. Searson, "On the influence of the nucleation overpotential on island growth in electrodeposition." *Electrochim. Acta*, **55**, 4086 (2010).

59. G. Whang, Q. Yan, D. Li, Z. Wei, D. Butts, P. Sautet, J. Luo, and B. Dunn, "Avoiding dendrite formation by confining lithium deposition underneath Li–Sn coatings." *J. Mater. Res.*, **36**, 797 (2021).

60. A. Hagopian, J. Touja, N. Louvain, L. Stievano, J.-S. Filhol, and L. Monconduit, "Importance of halide ions in the stabilization of hybrid sn-based coatings for lithium electrodes." *ACS Appl. Mater. Interfaces*, **14**, 10319 (2022).